A Computational Analysis of Nonlinear Fractional Partial Integro-differential Equation Using Meshfree Multiquadric Radial Basis Function Method

Arshed Ali[1*], Fasiha Shaheen[1], Imtiaz Ahmad[2], Hadia Atta[1]
[1]Department of Mathematics, Islamia College Peshawar, Pakistan.
[2]Institute of Informatics and Computing in Energy (IICE), Universiti Tenaga Nasional (UNITEN), Kajang, Selangor, Malaysia.
*__Correspondence__: arshad.ali@icp.edu.pk

Citation | Ali. A, Shaheen. F, Ahmad. I, Atta. H, "A Computational Analysis of Nonlinear Fractional Partial Integro-differential Equation Using Meshfree Multiquadric Radial Basis Function Method", IJIST, Vol. 7, Issue. 4 pp 3096-3111, December 2025
Received | November 07, 2025 **Revised |** November 24, 2025 **Accepted |** December 04, 2025 **Published |** December 10, 2025

Fractional partial integro-differential equations play an important role in describing physical and engineering systems that exhibit memory and nonlocal effects. Their nonlinear structure and the presence of weakly singular kernels make analytical solutions difficult to obtain, which highlights the need for accurate and flexible numerical strategies. This study develops a meshfree computational method based on multiquadric radial basis functions for solving a nonlinear fractional partial integro-differential equation involving the Caputo derivative. The temporal discretization is carried out using a backward difference formula, and the spatial operators are approximated through radial basis function interpolation. The resulting scheme avoids mesh generation and is suitable for irregular or scattered spatial nodes. Numerical experiments are presented to illustrate the accuracy, reliability, and efficiency of the method for representative test problems. The results indicate that the proposed meshfree approach provides a robust tool for nonlinear fractional models with weakly singular kernels.

Keywords: Fractional Partial Integro-Differential Equation; Caputo Derivative; Weakly Singular Kernel; Meshfree Method; Radial Basis Functions; Integral Operator.

Introduction:

Fractional calculus generalizes differentiation and integration to non-integer orders, offering mathematical operators that can model memory effects and hereditary properties in complex systems [1]. Unlike classical derivatives, fractional derivatives are nonlocal, as their evaluation at any given time depends on the entire history of the function. This nonlocal property makes them particularly suitable for modeling anomalous diffusion, viscoelasticity, relaxation processes, and multiscale transport phenomena [2][3]. Among the various definitions of fractional derivatives, the Caputo derivative is widely used in physical models because it accommodates classical initial conditions and possesses well-understood analytical properties [4]. The growing interest in fractional operators is linked to increasing experimental evidence that many natural and engineered systems display power-law memory, long-range interactions, and non-exponential relaxation, which cannot be captured accurately by integer-order models [5][6].

Fractional partial integro-differential equations (FPIDEs) appear naturally when fractional differentiation is combined with convolution-type integral operators representing additional memory effects [7][8]. Many fractional partial integro-differential equations (FPIDEs) involve weakly singular kernels, often of the form (t-s)^(α-1), which commonly appear in viscoelasticity, hereditary heat conduction, and population models with distributed delays [8][9][10][11]. Nonlinear FPIDEs are particularly difficult because they couple nonlocal differential operators, integral memory terms, and nonlinear reaction terms in a single framework [11][12][13][14][15]. The diversity of applications of nonlinear FPIDEs has stimulated the development of numerical strategies capable of handling nonlocal operators, memory integrals, and nonlinearities [9][11][12][13][14][15][16][17].

A wide range of numerical methods has been proposed by researchers to solve FPIDEs. For nonlinear FPIDEs, iterative schemes including Newton linearization, predictor–corrector techniques, fixed-point iterations, and Anderson-accelerated solvers have been used to enhance robustness and convergence behavior [11][12][13][16][17]. These grid-based methods have been successful; they often require structured meshes and may become less effective for irregular geometries, moving boundaries, or scattered spatial data sets.

Meshfree numerical methods have emerged as an effective alternative to classical grid-based schemes, as they eliminate the need for mesh generation and rely instead on scattered computational nodes to construct approximations [18]. These methods provide geometric flexibility, simplify local refinement, and allow the use of smooth basis functions that support accurate evaluation of higher order derivatives [19]. Commonly used meshfree techniques include the element-free Galerkin framework, moving least squares formulations, and radial basis function (RBF) interpolation [20]. Their ability to employ globally smooth functions makes them particularly suitable for fractional and integro-differential models where nonlocal operators require consistent approximation over extended spatial supports [21]. Recent developments in meshless theory further demonstrate their efficiency and robustness for a broad class of time-dependent and fractional PDEs. Examples include local differential quadrature formulations for PDEs [22], symmetric RBF schemes for elliptic problems [23], high-accuracy local meshless procedures for fractional PDEs arising in physics [24], and numerical simulation of multi-dimensional models using improved local meshless approaches [25]. Recent studies have also demonstrated the effectiveness of meshfree strategies for fractional viscous wave models with variable coefficients [26] and for highly complex nonlinear plasma and energy-related fractional PDE [27][28][29]. An increasing body of research shows that meshfree RBF-based methods provide a powerful and flexible framework for solving fractional partial integro-differential equations, especially

when handling scattered data, irregular geometries, derivative discontinuities, memory-dependent dynamics, or spatially nonlocal interactions [7].

Among meshfree techniques, radial basis function methods have shown strong performance for a variety of fractional partial differential equations due to their spectral-like accuracy and ability to approximate derivatives on scattered nodes [30]. Global RBFs such as Gaussian, multiquadric, and inverse multiquadric kernels provide smooth approximants that facilitate accurate computation of fractional and integral operators [31]. RBF collocation and RBF-based differential quadrature have been successfully applied to fractional diffusion, advection–diffusion, telegraph, and wave-diffusion equations in recent studies [25]. Extensions of RBF methods include local RBF collocation, hybrid RBF schemes, and spatio-temporal RBF formulations, which improve computational efficiency and conditioning while maintaining high accuracy [29]. These developments demonstrate that meshfree RBF methods provide a promising framework for solving nonlinear fractional partial integro-differential equations with weakly singular kernels, motivating the approach taken in the present article.

Although many numerical techniques have been developed for fractional partial integro-differential equations, several gaps remain in the existing literature. Most grid-based schemes rely on structured meshes and often lose accuracy when the solution involves strong nonlinearities or when spatial nodes are irregular or scattered. In addition, the presence of weakly singular kernels and memory-driven operators increases the difficulty of constructing stable and accurate approximations. These limitations motivate the need for meshfree strategies that can provide accurate derivative approximation, maintain stability for nonlinear models, and remain effective for scattered node distributions. The present study addresses these gaps by developing a multiquadric RBF-based method tailored for nonlinear FPIDEs with weakly singular kernels.

In this work, we consider the nonlinear FPIDE presented in equations (1)–(3) as follows:

$$\frac{\partial^{\alpha} v}{\partial t^{\alpha}} + v\frac{\partial v}{\partial \chi} - \int_0^t (t-p)^{\eta-1}\frac{\partial^2 v(\chi,p)}{\partial \chi^2}dp = G(\chi,t), t \geq 0 \quad (1)$$

$$v(\chi,0) = \varphi_0(\chi), \quad (2)$$

$$v(a,t) = \varphi_1(t),\ v(b,t) = \varphi_2(t)\ ,\ t \geq 0, \quad (3)$$

where $a \leq \chi \leq b, v = v(\chi,t), \frac{\partial^{\alpha}}{\partial t^{\alpha}}$ Denotes the α-order Caputo fractional derivative with $0 < \alpha \leq 1$, χ is the space variable, t is the time variable, and $\varphi_0, \varphi_1, \varphi_2, G(\chi,t)$ Given smooth functions.

This formulation encompasses a broad class of fractional evolution equations, where both memory-driven diffusion and hereditary integral effects influence the system dynamics. The initial and boundary conditions specified in equations (2) and (3) ensure the well-posedness of the problem and provide the foundation for the numerical treatment developed in the subsequent sections.

Objective:

This study presents a meshfree computational framework based on multiquadric radial basis functions (RBFs) for solving nonlinear fractional partial integro-differential equations (FPIDEs) with weakly singular kernels. The primary objective is to develop an accurate, flexible numerical scheme that circumvents the need for structured meshes, thereby efficiently handling problems with irregular geometries or scattered data. The novelty lies in the integration of a backward difference formula for Caputo derivative discretization with a global RBF interpolation for spatial and integral operators, specifically tailored to address the challenges posed by nonlinearity, memory effects, and weak singularities simultaneously. Through systematic numerical experiments, the work demonstrates the robustness, stability,

and high accuracy of the proposed method, offering a reliable computational tool for complex fractional models in science and engineering.

Methodology:

To construct the numerical scheme, the time interval $[0,T]$ is partitioned into uniform time levels $t_l = l\Delta t, l = 0,1,2,\dots,L$, and the spatial domain $[a,b]$ is divided by M nodes. The solution is then approximated at these discrete space–time points.

The following definitions provide the mathematical framework for the proposed technique.

Definition 1:

A function $\Phi: \mathbb{R}^n \to \mathbb{R}$ is referred to as *radial* when it can be written in the form

$$\Phi(\chi) = \psi(\|\chi\|),$$

where $\|.\|$ represents the Euclidean norm and $\psi: [0,\infty) \to \mathbb{R}$ is a single-variable function [30].

Definition 2:

An RBF is a real-valued function of one variable whose argument is the Euclidean distance from a prescribed center. For any node χ_j, the corresponding RBF takes the form

$$\psi_j(r) = \psi(\|\chi - \chi_j\|)$$

In this study, we employ the multiquadric (MQ) radial basis function, which is an infinitely smooth RBF given by [30]:

$$\boldsymbol{\psi(r_j) = \sqrt{r_j^2 + c^2}},$$

where $r_j = \|\chi - \chi_j\|$ and $c > 0$ is the shape parameter. The choice of c influences both the accuracy of the approximation and the conditioning of the resulting system [30].

Definition 3:

The Caputo derivative $\frac{\partial^\alpha v(\chi,t)}{\partial t^\alpha}$ The order α has the following form [10]:

$$\frac{\partial^\alpha v(\chi,t)}{\partial t^\alpha} = \frac{1}{\Gamma(1-\alpha)} \int_0^t (t-q)^{-\alpha} \frac{\partial v(\chi,q)}{\partial q} dq, \quad (4)$$

where $0 \le \alpha \le 1$.

Approximation in Time:

To develop the proposed technique, we take $t = t_{N+1}$ in Eq. (1),

$$\frac{\partial^\alpha v(\chi,t_{N+1})}{\partial t^\alpha} + v(\chi,t_{N+1}) \frac{\partial v(\chi,t_{N+1})}{\partial \chi} - \int_0^{t_{N+1}} (t_{N+1}-p)^{\eta-1} \frac{\partial^2 v(\chi,p)}{\partial \chi^2} dp = G(\chi,t_{N+1}), \quad (5)$$

For the Caputo derivative appearing in (5), the corresponding backward difference approximation of the truncation error $R_{\Delta t}^{N+1}$ is given by [10]:

$$\frac{\partial^\alpha v(\chi,t_{N+1})}{\partial t^\alpha} = \frac{1}{\Gamma(2-\alpha)} \sum_{l=0}^{N} c_l \frac{v(\chi,t_{N+1-l}) - v(\chi,t_{N-l})}{(\Delta t)^\alpha} + R_{\Delta t}^{N+1}, \quad (6)$$

where $c_l = (l+1)^{1-\alpha} - l^{1-\alpha}, l = 0,1,2,\dots,N$, and $R_{\Delta t}^{N+1} \le C_v \Delta t^{2-\alpha}$.

The integral term in Eq. (5) is approximated as follows:

$$\int_0^{t_{N+1}} (t_{N+1}-p)^{\eta-1} \frac{\partial^2 v(\chi,p)}{\partial \chi^2} dp = \int_0^{t_{N+1}} p^{\eta-1} \frac{\partial^2 v(\chi,t_{N+1}-p)}{\partial \chi^2} dp,$$

$$= \sum_{l=0}^{N} \int_{t_l}^{t_{l+1}} p^{\eta-1} \frac{\partial^2 v(\chi,t_{N+1}-p)}{\partial \chi^2} dp,$$

Taking $p = t_l$ in $\frac{\partial^2 v(\chi,t_{N+1}-p)}{\partial \chi^2}$, we get

$$= \sum_{l=0}^{N} \frac{\partial^2 v(\chi, t_{N+1} - t_l)}{\partial \chi^2} \int_{t_l}^{t_{l+1}} p^{\eta-1} dp,$$

$$= \frac{\Delta t^\eta}{\eta} \sum_{l=0}^{N} \frac{\partial^2 v(\chi, t_{N+1} - t_l)}{\partial \chi^2} ((l+1)^\eta - l^\eta),$$

$$= \frac{\Delta t^\eta}{\eta} \sum_{l=0}^{N} d_l \frac{\partial^2 v(\chi, t_{N+1-l})}{\partial \chi^2}, \qquad (7)$$

where $d_0 = 1, d_l = (l+1)^\eta - l^\eta,\ l = 1,2,\dots,N.$

The nonlinear term $v(\chi, t_{N+1}) \frac{\partial v(\chi, t_{N+1})}{\partial \chi}$ in Eq. (5) is linearized by the following formula,

$$v(\chi, t_{N+1}) \frac{\partial v(\chi, t_{N+1})}{\partial \chi} = v(\chi, t_N) \frac{\partial v(\chi, t_{N+1})}{\partial \chi} + v(\chi, t_{N+1}) \frac{\partial v(\chi, t_N)}{\partial \chi} - v(\chi, t_N) \frac{\partial v(\chi, t_N)}{\partial \chi}. \quad (8)$$

Thus, using Eqs. (6)-(8) in (5) and rearranging, we have

$$v^{N+1}(\chi) + \Delta t^\alpha \Gamma(2-\alpha) \left(v_\chi^N(\chi) v^{N+1}(\chi) + v^N(\chi) v_\chi^{N+1}(\chi) - \frac{\Delta t^\eta}{\eta} v_{\chi\chi}^{N+1}(\chi) \right)$$
$$= \Delta t^\alpha \Gamma(2-\alpha) v^N(\chi) v_\chi^N(\chi) + c_N v^0(\chi) + (1 - c_1) v^N(\chi)$$
$$+ \sum_{l=1}^{N-1} (c_l - c_{l+1}) v^{N-l}(\chi) + \frac{\Delta t^{\alpha+\eta}}{\eta} \Gamma(2-\alpha) \sum_{l=1}^{N} d_l v_{\chi\chi}^{N+1-l}(\chi)$$
$$+ \Delta t^\alpha \Gamma(2-\alpha) G^{N+1}(\chi), \qquad (9)$$

where $v^N(\chi) = v(\chi, t_N), v_\chi^N(\chi) = \frac{\partial v(\chi, t_N)}{\partial \chi}$ and $G^{N+1}(\chi) = G(\chi, t_{N+1}).$

For $\chi = \chi_i$, Eq. (9) becomes

$$v^{N+1}(\chi) + \Delta t^\alpha \Gamma(2-\alpha) \left(v_\chi^N(\chi) v^{N+1}(\chi) + v^N(\chi) v_\chi^{N+1}(\chi) - \frac{\Delta t^\eta}{\eta} v_{\chi\chi}^{N+1}(\chi) \right)$$
$$= H_i, \qquad (10)$$

where

$$H_i = \Delta t^\alpha \Gamma(2-\alpha) v^N(\chi_i) v_\chi^N(\chi_i) + c_N v^0(\chi_i) + (1 - c_1) v^N(\chi_i)$$
$$+ \sum_{l=1}^{N-1} (c_l - c_{l+1}) v^{N-l}(\chi_i) + \frac{\Delta t^{\alpha+\eta}}{\eta} \Gamma(2-\alpha) \sum_{l=1}^{N} d_l v_{\chi\chi}^{N+1-l}(\chi_i)$$
$$+ \Delta t^\alpha \Gamma(2-\alpha) G^{N+1}(\chi_i).$$

Approximation in Space:

The RBF approximation of the function $v^{N+1}(\chi)$ at $\chi = \chi_i, i = 1,2,\dots,L$ is given by

$$v^{N+1}(\chi_i) = \sum_{j=1}^{M} \lambda_j^{N+1} \psi(r_{ij}), \quad (11)$$

where $r_{ij} = \|\chi_i - \chi_j\|.$

Thus for $i = 2,3,\dots,M-1,$ Eqs. (10) and (11) provide

$$\sum_{j=1}^{M} \lambda_j^{N+1} \psi(r_{ij}) + \Delta t^{\alpha}\, \Gamma(2-\alpha) \left(\sum_{j=1}^{M} \lambda_j^{N} \psi'(r_{ij}) \sum_{j=1}^{M} \lambda_j^{N+1} \psi(r_{ij}) + \sum_{j=1}^{M} \lambda_j^{N+1} \psi'(r_{ij}) \sum_{j=1}^{M} \lambda_j^{N} \psi(r_{ij}) - \frac{\Delta t^{\eta}}{\eta} \sum_{j=1}^{M} \lambda_j^{N+1}\, \psi''(r_{ij}) \right) = H_i. \quad (12)$$

For $i = 1, M$, Eq. (3) leads to

$$\sum_{j=1}^{M} \lambda_j^{N+1} \psi(r_{ij}) = \varphi_1(t^{N+1}) \quad (13)$$

and

$$\sum_{j=1}^{M} \lambda_j^{N+1} \psi(r_{ij}) = \varphi_2(t^{N+1}), \quad (14)$$

Respectively.

Eqs. (12)-(14) are represented in matrix form as follows:

$$\left(\mathbf{A} + \Delta t^{\alpha}\, \Gamma(2-\alpha)\left(\mathbf{v}^{N} * \mathbf{B} + \mathbf{v}_{\chi}^{N} * \mathbf{C}\right) - \frac{\Delta t^{\alpha+\eta}}{\eta}\, \Gamma(2-\alpha)\mathbf{D}\right) \boldsymbol{\lambda}^{N+1} = \mathbf{H}, \quad (15)$$

Where $\mathbf{A}, \mathbf{B}, \mathbf{C}$ are $M \times M$ matrices and $\mathbf{v}^{N}, \mathbf{v}_{\chi}^{N}$ Are $M \times 1$ matrices such that $\mathbf{A} = [\psi(r_{ij}): 1 \le i, j \le M]$, $\mathbf{B} = [\psi'(r_{ij}): 2 \le i \le M-1, 1 \le j \le M, \text{and 0 elsewhere}]$, $\mathbf{C} = [\psi(r_{ij}): 2 \le i \le M-1, 1 \le j \le M \text{ and 0 elsewhere}]$, $\mathbf{v}^{N} = [v^{N}(\chi_i): 1 \le i \le M]$, $\mathbf{v}_{\chi}^{N} = [v_{\chi}^{N}(\chi_i): 1 \le i \le M]$, $\mathbf{H} = [\varphi_1(t^{N+1}), H_2, H_3, \dots, H_{M-1}, \varphi_2(t^{N+1})]$ and $\boldsymbol{\lambda}^{N+1} = [\lambda_i^{N+1}: 1 \le i \le M]$.

Algorithm:

The numerical scheme in (15) can be carried out through the following sequence of steps:

Selection of spatial nodes:

Choose M collocation points in the spatial interval $[a, b]$ that will be used for constructing the RBF approximation.

Time Discretization:

Fix the time step Δt and determine the discrete time levels. $t_l = l\Delta t, l = 0,1,2, \dots, L$.

Computation of RBF quantities:

Specify the multiquadric radial basis function $\psi(r)$ and evaluate all matrices and vectors that appear in the discrete formulation in Eq. (15).

Initialization and first solve:

Use the initial condition from Eq. (2) to obtain the coefficients $\boldsymbol{\lambda}^{0}$.

Then solve the system in Eq. (15) to compute the solution at the first time level.

Time marching:

For each successive step N, update the coefficients $\boldsymbol{\lambda}^{N+1}$ by solving Eq. (15) and evaluating the approximate solution using Eq. (11).

The flow diagram of the algorithm is given as:

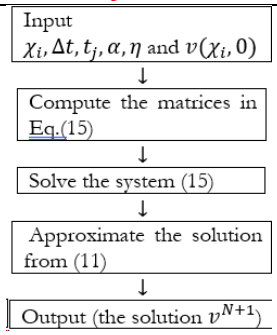

Stability Analysis:

The stability of the proposed meshfree scheme is investigated using a perturbation approach. We examine how errors in the initial data propagate through the time-stepping procedure. The following theorem establishes a sufficient condition for numerical stability.

Theorem 1 (Stability):

Consider the numerical scheme defined by Eq. (15). Assume the exact solution $v(\chi, t)$ is sufficiently smooth and the multiquadric RBF shape parameter cc is chosen such that the system matrices are well-conditioned. If the time step Δt satisfies the condition

$$\Delta t^{\alpha}\, \Gamma(2-\alpha)(\| \boldsymbol{v}_{\chi}^{N} \|_{\infty} + \| \boldsymbol{v}^{N} \|_{\infty} \| L' \|) \leq \kappa < 1,$$

where L' is the spatial differential operator associated with the RBF approximation, then the scheme is unconditionally stable in the sense that a small perturbation in the initial data leads to a bounded perturbation in the numerical solution at later times.

Proof. Let $\tilde{v}^N$ Be the perturbed numerical solution at time level N, and define the error. $e^N = v^N - \tilde{v}^N$. Substituting into the linearized discrete equation (10) and subtracting the perturbed equation, we obtain an error evolution equation. Under the linearization (8) and using the properties of the Caputo derivative discretization [10], the error satisfies

$$(1 + \Delta t^{\alpha}\Gamma(2-\alpha)L_N)e^{N+1} = \sum_{l=0}^{N-1} \beta_l e^{N-1} + \Delta t^{\alpha+\eta}\gamma \sum_{l=1}^{N} d_l\, L_{\chi\chi} e^{N+1-l},$$

where L_N is a linear operator depending on v^N and v_{χ}^N, and β_l, γ are constants derived from the discretization weights. Taking norms and applying Gronwall's inequality for discrete systems [11], we find

$$\| e^{N+1} \| \leq C \| e^{0} \| \; for\; all\; N \geq 0,$$

provided the condition on Δt holds. The constant C depends on $\alpha, \eta, T,$ and the stability constants of the RBF interpolation matrices [30]. This demonstrates that initial errors do not grow unboundedly, ensuring numerical stability.

Remarks:

The condition in Theorem 1 is mild and is typically satisfied for moderate time steps, as observed in the numerical experiments where stable results were obtained for all tested values of Δt.

Convergence Analysis:

The convergence of the proposed method is analysed by estimating the truncation error and examining its behavior as the spatial and temporal step sizes approach zero. The following theorem provides the convergence rate.

Theorem 2 (Convergence):

Let $v(\chi, t) \in C^{4,2}([a, b] \times [0, T])$ be the exact solution of the nonlinear FPIDE (1)–(3), and let $v_{h,\Delta t}$ be the numerical solution obtained by the scheme (15) using multiquadric RBFs with shape parameter cc and uniform time step Δt. Assume the stability

condition of Theorem 1 holds. Then, there exist constants $C_1, C_2 > 0$, independent of h and Δt, such that the global error satisfies

$$\| v(\cdot, t_N) - v_{h,\Delta t}(\cdot, t_N) \|_{L_\infty} \leq C_1 \Delta t^{2-\alpha} + C_2 h^{m(c)},$$

Where $m(c) > 0$ is the convergence order of the multiquadric RBF interpolation, which depends on the shape parameter c and the smoothness of the solution [30].

Proof. The global error at time t_N Is decomposed into temporal and spatial components:

$$E^N = v(\cdot, t_N) - v_{h,\Delta t}(\cdot, t_N) = \underbrace{\left(v(\cdot, t_N) - v_{\Delta t}(\cdot, t_N)\right)}_{Temporal\ Error} + \underbrace{\left(v_{\Delta t}(\cdot, t_N) - v_{h,\Delta t}(\cdot, t_N)\right)}_{Spatial\ Error}.$$

Temporal Error:

The Caputo derivative is approximated by the $L1$-formula with local truncation error $O(\Delta t^{2-\alpha})$ [10][11]. By the stability, the accumulation of the local errors over N steps yields a global temporal error bound $O(\Delta t^{2-\alpha})$.

Spatial Error:

The spatial approximation uses multiquadric RBF interpolation. For a sufficiently smooth solution, the error between the exact solution and its RBF interpolant at the collocation nodes satisfies [30][31]

$$\| v(\cdot, t) - \Pi_h v(\cdot, t) \|_{L_\infty} \leq F(c)\, h^{m(c)},$$

where Π_h is the RBF interpolation operator, h is the nodal spacing, and $F(c)$ is a function of the shape parameter. The spatial derivatives in the scheme are approximated via differentiation of the RBF interpolant, preserving this convergence order for the differential operators [30].

Combining the bounds for temporal and spatial errors via the triangle inequality and using the stability of the scheme (which ensures error propagation is controlled), we obtain the stated global error estimate.

Test Problems Used for Numerical Validation:

Test Example-1:

We take the FPIDE with $v(\chi, 0) = \sin(\pi\chi)\,, \chi \in [0, 1]$ and

$$G(\chi, t) = \pi\left(\frac{\pi}{\eta}t^\eta - 4t^3\cos(2\pi\chi)\right)\sin(\pi\chi) + \left(\frac{\pi}{2} - \frac{12}{\Gamma(4-\eta)}t^{3-\alpha} - 2\pi t^3\cos(\pi\chi) - \frac{48\pi^2\Gamma(\eta)}{\Gamma(\eta+4)}t^{3+\eta}\right) + (8\pi t^6\cos(2\pi\chi)\sin(2\pi\chi)).$$

The analytic solution is given by [11]:

$v(\chi, t) = \sin(\pi\chi) - 2t^3\sin(2\pi\chi)$.

Test Example-2:

Consider the model problem (1) with the initial condition and source term as shown below [11]:

$$v(\chi, 0) = \chi^2(1-\chi)^2,$$

$$G(\chi, t) = \frac{\Gamma\left(\frac{7}{3}\right)}{\Gamma\left(\frac{7}{2} - \alpha\right)}t^{\frac{5}{2}-\alpha}\chi^2(1-\chi)^2 - 2\left(\frac{1}{\eta}t^\eta + \frac{\Gamma\left(\frac{7}{3}\right)\Gamma(\eta)}{\Gamma\left(\frac{7}{2}\right) + \eta}\right)(1 - 6\chi + 6\chi^2) + 2\left(1 + t^{\frac{5}{2}}\right)^2(1-2\chi)\chi^3(1-\chi)^3,$$

An analytical solution is $v(\chi, t) = \left(1 - t^{\frac{5}{7}}\right)\chi^2(1-\chi)^2$.

Numerical Experiments, Results, and Discussion:

Numerical experiments were conducted to evaluate the performance of the proposed scheme given in Eq. (15). Two test problems defined on the spatial interval [0,1] were considered to validate the accuracy and stability of the approach. The accuracy of the

numerical results was measured using the L_∞ and L_2 error norms. For each example, the functions $\varphi_0(\chi), \varphi_1(t),$ and $\varphi_2(t)$ Were derived directly from the corresponding analytical solution. The values of the shape parameter c that produced the most accurate approximations are reported in the accompanying tables. However, accuracy can be further improved by varying the value of the shape parameter c. All computations were performed using uniformly spaced spatial nodes on a system equipped with 2 GB RAM and an Intel Core i3 2.4 GHz processor.

Numerical simulations for Example 1 were carried out for different values of the fractional parameters α and η, the spatial step size h, and the time step Δt. The computed results are summarized in Tables 1–3. Table 1 presents the values of L_∞, L_2 and the temporal rate of convergence for several time step sizes using $\alpha = 0.5, h = \frac{1}{32}, t = 1$, and $\eta = 0.15$. The results are compared with the method reported in [11], and it is clear that the proposed method provides better accuracy. Similarly, in Table 2, we again compare the results of the proposed method with the method reported in [11] in terms of L_∞ and L_2 for various values of h and $\Delta t = \frac{1}{1000}, \eta = 0.15, t = 1.$ In Tables 1 and 2, the last two columns present the rate of convergence (ROC) using L_2 and the computational time (RT), providing a quantitative measure of the efficiency of the proposed scheme. The ROC values in Table 1 approach the expected theoretical order [11] as the time step Δt is refined, confirming the temporal accuracy and stability of the method, while the corresponding CPU times remain low and increase only moderately. Likewise, Table 2 exhibits consistent convergence rates with decreasing spatial step size h, and the gradual rise in computational time reflects good scalability.

Table 3 presents the absolute errors at selected spatial points for various values of α, illustrating the influence of the fractional order. The results indicate that the method achieves reasonably good accuracy. Overall, the errors remain small throughout the domain, and their variation with α reflects the expected memory effects inherent in fractional models. Shape parameters $c = 0.1, 0.065, 0.12, 0.15$ were used for $\alpha = 0.25, 0.5, 0.75, 0.95$, respectively, to ensure accurate solutions.

Table 4 highlights the influence of the fractional order η on the solution behavior. The results indicate that changes in η significantly affect the magnitude of the numerical errors at selected spatial points. In particular, larger values of η tend to introduce stronger fractional damping effects, which modify both the solution amplitude and convergence characteristics. These observations further confirm that η plays an important role in governing the memory and diffusion properties of the underlying fractional model. The influence of the fractional orders α and η on the solution behavior is evident from the numerical results. As α increases, the solution becomes smoother, and the errors at selected spatial points generally decrease, reflecting the stronger memory effect associated with higher fractional orders. Variations in η affect both the solution amplitude and convergence rate, with larger values leading to slightly slower temporal evolution due to enhanced fractional damping. These trends demonstrate that α and η play a critical role in controlling the memory and diffusion characteristics of the system, and their appropriate selection is essential for accurately capturing the system dynamics. Figures 1–3 illustrate the results for Example 1. In particular, Figure 1 shows a comparison between the exact and approximate solutions at $t = 1$, demonstrating strong agreement. Figure 2 presents the corresponding error profile, while Figure 3 provides a three-dimensional view of the approximate solution, confirming the scheme's stability and accuracy.

Table 1. $h = \frac{1}{32}, \eta = 0.15, t = 1$

α	Δt	c	L_2 [11]	L_2	ROC	RT(sec)
0.50	1/4	0.07	1.3017e-02	1.8508e-04	---	0.03016
0.50	1/8	0.09865	5.0567e-03	6.6737e-05	1.4716	0.03282
0.50	1/16	0.13948	1.1256e-03	2.3831e-05	1.4856	0.04181
0.50	1/32	0.175485	3.0480e-04	8.4722e-06	1.4920	0.06121

Table 2. $\Delta t = \frac{1}{1000}, \eta = 0.15, t = 1$

α	h	c	L_2 [11]	L_2	ROC	RT(sec)
0.50	$1/4$	0.72	2.2193e-01	1.0484e-04	---	0.24115
0.50	$1/8$	0.5456	4.5644e-02	2.0067e-05	2.3853	0.43763
0.50	$1/16$	0.3928	5.8752e-03	3.6854e-06	2.4449	0.89671
0.50	$1/32$	0.21033	6.8860e-04	6.7443e-07	2.4501	1.95560

Table 3. $N = 100, \Delta t = \frac{1}{100}, \eta = 0.05, t = 1$

χ	$\alpha = 0.25$	$\alpha = 0.5$	$\alpha = 0.75$	$\alpha = 0.95$
0.1	1.1597e-003	7.3176e-004	3.3751e-004	2.4908e-003
0.2	1.8762e-003	1.2421e-003	5.4718e-004	3.9469e-003
0.3	1.8787e-003	1.2627e-003	5.5845e-004	4.3152e-003
0.4	1.1718e-003	7.9490e-004	3.7903e-004	2.4768e-003
0.5	2.5986e-005	2.4771e-005	8.2508e-005	1.6451e-005
0.6	1.1263e-003	7.4815e-004	2.2276e-004	2.4454e-003
0.7	1.8489e-003	1.2218e-003	4.4707e-004	4.1078e-003
0.8	1.8625e-003	1.2047e-003	4.5323e-004	4.3342e-003
0.9	1.1557e-003	6.9165e-004	2.8897e-004	2.8704e-003

Table 4. $N = 100, \Delta t = \frac{1}{100}, \alpha = 0.5, c = 0.025, t = 1$

χ	$\eta = 0.25$	$\eta = 0.5$	$\eta = 0.75$	$\eta = 0.95$
0.1	2.7464e-003	3.8540e-003	8.8542e-004	7.6614e-003
0.2	5.6792e-003	6.8822e-003	1.3939e-003	2.1993e-002
0.3	5.9582e-003	6.4805e-003	3.3960e-004	2.7384e-002
0.4	3.8467e-003	3.7238e-003	7.3330e-004	2.2319e-002
0.5	3.5661e-004	1.3600e-004	1.2919e-003	1.3630e-002
0.6	3.1837e-003	4.0959e-003	1.4176e-003	5.0971e-003
0.7	5.3851e-003	7.0775e-003	1.4589e-003	2.5843e-003
0.8	5.0877e-003	7.5303e-003	1.5532e-003	7.4358e-003
0.9	1.9138e-003	3.8967e-003	4.1638e-004	5.6963e-003

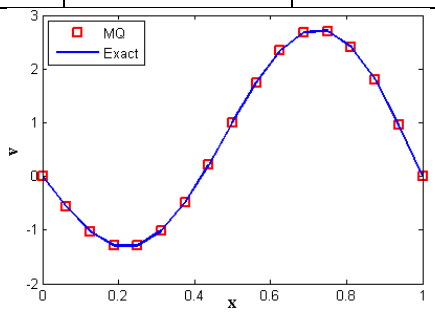

Figure 1. Plots of Exact and approximate solutions at $t = 1$ for $\Delta t = {}^{1}/_{16}, N = 16, \alpha = 0.5, \eta = 0.01$ corresponding to Test Example-1

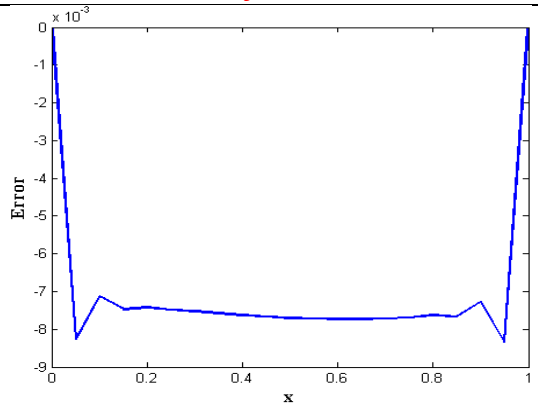

Figure 2. Error in approximate solution at $t = 1$ using $\Delta t = {}^{1}/_{16}, N = 16, \alpha = 0.5, \eta = 0.01$ corresponding to Test Example-1.

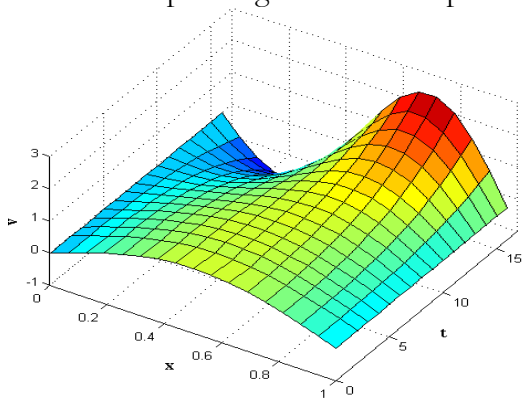

Figure 3. 3D Surface plot of approximate solutions over the domain $[0, 1] \times [0, 1]$for $\Delta t = {}^{1}/_{16}, N = 16, \alpha = 0.5, \eta = 0.01$ corresponding to Test Example-1.

Numerical simulations for Example 2 were performed for different values of α, η, h, and Δt. The computed results are presented in Tables 5–8. Table 5 provides a comparison of the proposed method in comparison with the method in [29] in terms of L_∞, L_2, for $\alpha = 0.25, 0.5$ and for several time step sizes Δt using $h = \frac{1}{32}, \eta = 0.15, t = 1$. It is clear that the proposed method provides good accuracy. Similarly, in Table 6, the results are compared with the method reported in [11] for various values of h, and the proposed method is found to be more accurate in this case. In Table 5, the ROC values obtained using L_2 are given for different values of the fractional order α as Δt decreases, confirming the temporal accuracy of the proposed method [11]. The computational time increases moderately with time-step refinement, indicating that higher accuracy is achieved without excessive computational overhead. Similarly, Table 6 shows stable and consistent ROC values under spatial refinement, demonstrating reliable spatial convergence. Although the RT increases for finer meshes, this behavior is expected and reflects the increased resolution rather than a loss of efficiency. Overall, Tables 5 and 6 confirm that the proposed scheme is both accurate and computationally efficient. Table 7 lists the absolute errors at selected spatial points for different α values. Table 8 illustrates the effect of the fractional order η on the solution behavior. An increase in η leads to larger solution magnitudes across the domain, highlighting the enhanced memory effects associated with higher fractional orders. These results confirm the sensitivity of the model to η and demonstrate the capability of the proposed method to capture fractional-order dynamics accurately. Example 2 exhibits oscillatory behavior and heightened sensitivity to the fractional parameters. The results in Tables 5–8 further demonstrate the robustness and reliability of the proposed scheme.

Figures 4–6 provided visual confirmation of these findings. Figure 4 compared the exact and computed solutions at $t = 1$ and demonstrated strong agreement. Figure 5 illustrates the error structure, and Figure 6 presents the approximate solutions for finer meshes with $N = 16$, confirming the numerical stability and accuracy of the method across the entire domain over time.

Table 5. $h = \frac{1}{32}, \eta = 0.15, t = 1$

α	Δt	c	L_∞ [29]	L_2 [29]	L_∞	L_2	ROC	RT(sec)
0.25	$1/4$	0.0571	5.0619e-03	1.0233e-04	2.95e-03	1.48e-03	---	0.0534
0.25	$1/8$	0.0385	1.5075e-03	3.1934e-04	1.01e-03	4.42e-04	1.7459	0.0569
0.25	$1/16$	0.0427	4.4568e-04	8.5420e-05	2.67e-04	1.31e-04	1.7579	0.0912
0.25	$1/32$	0.03563	1.3363e-04	1.8820e-06	2.73e-04	3.87e-05	1.7535	0.1485
0.50	$1/4$	0.0565	5.0551e-03	1.0218e-04	3.12e-03	1.59e-03	---	0.0524
0.50	$1/8$	0.0427	1.5101e-03	3.1976e-05	1.04e-03	4.84e-04	1.7173	0.0669
0.50	$1/16$	0.03915	4.5565e-04	8.1780e-06	4.06e-04	1.46e-04	1.7322	0.0917
0.50	$1/32$	0.03854	1.3491e-04	1.9550e-06	2.52e-04	4.34e-05	1.7460	0.1420

Table 6. $\Delta t = \frac{1}{1000}, \eta = 0.15, c = 0.2, t = 1$

α	h	c	L_∞ [11]	L_2 [11]	L_∞	L_2	ROC	RT(sec)
0.50	$1/4$	16	5.4935e-02	1.8224e-02	8.39e-05	4.96e-05	---	0.4306
0.50	$1/8$	1.79	1.3643e-02	3.4518e-03	2.45e-05	9.89e-06	2.4479	0.9301
0.50	$1/16$	0.598	3.3125e-03	7.8340e-04	2.01e-05	1.62e-06	2.4891	1.9183
0.50	$1/32$	0.2018	8.0164e-04	2.5050e-05	2.77e-05	2.90e-07	2.4830	4.1079

Table 7. $N = 1000, \Delta t = \frac{1}{32}, \eta = 0.15, c = 0.2, t = 1$

χ	$\alpha = 0.25$	$\alpha = 0.5$	$\alpha = 0.75$	$\alpha = 0.95$
0.1	7.7069e-006	6.8124e-005	2.3609e-004	4.8442e-004
0.2	6.4604e-005	8.3152e-005	4.1054e-004	8.9481e-004
0.3	1.3171e-004	7.6427e-005	5.3774e-004	1.2204e-003
0.4	1.8241e-004	6.6277e-005	6.1756e-004	1.4336e-003
0.5	2.0114e-004	6.2055e-005	6.4555e-004	1.5093e-003
0.6	1.8274e-004	6.6571e-005	6.1924e-004	1.4373e-003
0.7	1.3221e-004	7.6909e-005	5.4037e-004	1.2262e-003
0.8	6.5032e-005	8.3640e-005	4.1303e-004	9.0021e-004
0.9	7.9323e-006	6.8423e-005	2.3753e-004	4.8753e-004

Table 8. $N = 100, \Delta t = \frac{1}{100}, \alpha = 0.5, c = 0.02, t = 1$

χ	$\eta = 0.25$	$\eta = 0.5$	$\eta = 0.75$	$\eta = 0.95$
0.1	5.5279e-005	1.7380e-004	3.8309e-004	4.6193e-004
0.2	7.6605e-005	2.6963e-004	6.5911e-004	8.1456e-004
0.3	7.3528e-005	3.1499e-004	8.5071e-004	1.0866e-003
0.4	6.5310e-005	3.3590e-004	9.7241e-004	1.2882e-003
0.5	6.1656e-005	3.4331e-004	1.0227e-004	1.4018e-003
0.6	6.5498e-005	3.3964e-004	9.9589e-004	1.3997e-003
0.7	7.3883e-005	3.2109e-004	8.8797e-004	1.2610e-003

0.8	7.7022e-005	2.7576e-004	6.9513e-004	9.7974e-004
0.9	5.5560e-005	1.7752e-004	4.0430e-004	5.5740e-004

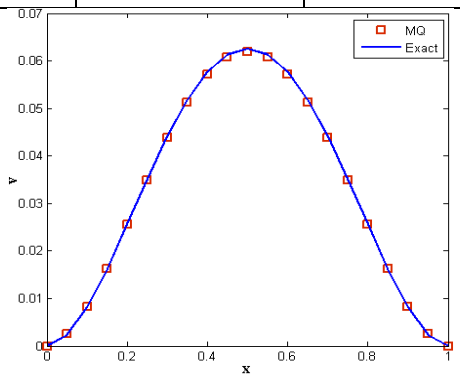

Figure 4. Plots of Exact and approximate solutions at $t = 1$ for $\Delta t = {}^{1}/_{16}, N = 20, \alpha = 0.5,\ \eta = 0.05$ corresponding to Test Example-2

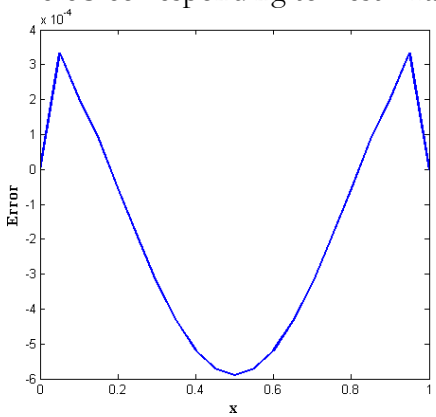

Figure 5. Error in approximate solution at $t = 1$ using $\Delta t = {}^{1}/_{16}, N = 16, \alpha = 0.5, \eta = 0.05$ corresponding to Test Example-2.

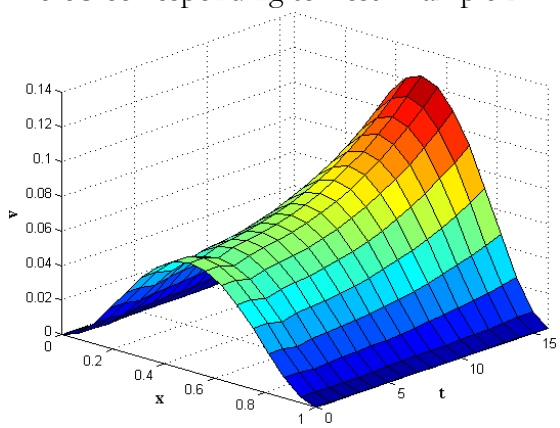

Figure 6. 3D Surface plot of approximate solutions over the domain $[0, 1] \times [0, 1]$for $\Delta t = {}^{1}/_{16}, N = 16, \alpha = 0.5, \eta = 0.05$ corresponding to Test Example-2

Conclusion:

This work presented a mesh-free numerical framework based on multiquadric radial basis functions for solving a nonlinear fractional partial integro-differential equation with a weakly singular kernel. The method combined a backward difference approximation for the Caputo derivative with RBF interpolation for the spatial and integral operators, which allowed the full scheme to be implemented without any need for structured meshes. Numerical experiments demonstrated that the proposed approach provides accurate

approximations for representative test problems. The computed solutions showed close agreement with the analytical solutions across the spatial domain, and the error norms confirmed the reliability and efficiency of the method for different fractional parameters and discretization settings. These findings indicate that the meshfree multiquadric RBF strategy is a useful computational tool for fractional models involving memory effects and nonlinearities. The approach can be extended to higher-dimensional problems and to other classes of fractional integro-differential equations in future studies.

Author's Contribution:

Conceptualization: Arshed Ali and Fasiha Shaheen; Data curation: Fasiha and Imtiaz Ahmad; Formal analysis: Imtiaz Ahmad and Hadia Atta; Investigation: Hadia Atta and Fasiha Shaheen; Methodology: Arshed Ali and Fasiha Shaheen; Supervision: Arshed Ali; Validation: Arshed Ali and Fasiha Shaheen; Software: Hadia Atta and Fasiha Shaheen; Writing original draft: Fasiha Shaheen; Resources: Arshed Ali and Imtiaz Ahmad; Writing review & editing: Arshed Ali and Hadia Atta.

Conflict of Interest: The authors declare that they have no competing interests in publishing this manuscript in IJIST.

References:

[1] I. Podlubny, "Fractional Differential Equation," *Math. Sci. Eng.*, vol. 198, 1999, [Online]. Available: https://www.researchgate.net/publication/249993249_Fractional_Differential_Equations_and_Their_Applications

[2] J. L. Suzuki, M. Gulian, M. Zayernouri, and M. D'Elia, "Fractional Modeling in Action: a Survey of Nonlocal Models for Subsurface Transport, Turbulent Flows, and Anomalous Materials," *J. Peridynamics Nonlocal Model. 2022 53*, vol. 5, no. 3, pp. 392–459, Oct. 2022, doi: 10.1007/S42102-022-00085-2.

[3] I. A. Imtiaz Ahmad, "Solutions of a three-dimensional multi-term fractional anomalous solute transport model for contamination in groundwater," *plos one*, 2023, doi: https://doi.org/10.1371/journal.pone.0294348.

[4] D. B. Zaid Odibat, "On a New Modification of the Erdélyi–Kober Fractional Derivative," *Fractal Fract*, vol. 5, no. 3, p. 121, 2021, doi: https://doi.org/10.3390/fractalfract5030121.

[5] A. A. B. Imtiaz Ahmad, "Investigating Virus Spread Analysis In Computer Networks With Atangana–Baleanu Fractional Derivative Models," *Fractals*, vol. 32, 2024, doi: https://doi.org/10.1142/S0218348X24400437.

[6] R. A. K. Arshed Ali, "A Computational Simulation of Fractional Advection-Diffusion Model Using Differential Quadrature and Local Radial Basis Functions," *Int. J. Agric. Sustain. Dev.*, vol. 7, no. 2, 2025, doi: 10.33411/ijist/202572926938.

[7] Imtiaz Ahmad, Arshed Ali, "An Efficient RBF-Based Collocation Approach for Second-Order Fractional Partial Integro-Differential Problems with Singular Kernel," *J. Appl. Comput. Mech.*, 2025, doi: 10.22055/jacm.2025.48574.5336.

[8] S. Zaeri, H. Saeedi, and M. Izadi, "Fractional integration operator for numerical solution of the integro-partial time fractional diffusion heat equation with weakly singular kernel," *https://doi.org/10.1142/S1793557117500711*, vol. 10, no. 4, Oct. 2017, doi: 10.1142/S1793557117500711.

[9] S. Arshed, "B-spline solution of fractional integro partial differential equation with a weakly singular kernel," *Numer. Methods Partial Differ. Equ.*, vol. 33, no. 5, pp. 1565–1581, Sep. 2017, doi: 10.1002/NUM.22153; JOURNAL:10982426;WGROUP:STRING:PUBLICATION.

[10] H. K. Mehwish Saleem, Arshed Ali, Fazal-i-Haq, "Numerical approximation of time-fractional nonlinear partial integro-differential equation using fractional Euler and

cubic trigonometric B-Spline methods," *Partial Differ. Equations Appl. Math.*, vol. 15, p. 101223, 2025, doi: https://doi.org/10.1016/j.padiff.2025.101223.

[11] Z. A. Tayyaba Akram, "A Numerical Study of Nonlinear Fractional Order Partial Integro-Differential Equation with a Weakly Singular Kernel," *Fractal Fract*, vol. 5, no. 3, p. 85, 2021, doi: https://doi.org/10.3390/fractalfract5030085.

[12] J. Guo, D. Xu, and W. Qiu, "A finite difference scheme for the nonlinear time-fractional partial integro-differential equation," *Math. Methods Appl. Sci.*, vol. 43, no. 6, pp. 3392–3412, Apr. 2020, doi: 10.1002/MMA.6128;SUBPAGE:STRING:ABSTRACT;WEBSITE:WEBSITE:PERICLES;ISSUE:ISSUE:DOI.

[13] T. A. Imtiaz Ahmad, Mehwish Saleem, Arshed Ali, Aziz Khan, "A Computational Analysis of Convection-Diffusion Model with Memory using Caputo-Fabrizio Derivative and Cubic Trigonometric B-Spline Functions," *Eur. J. Pure Appl. Math.*, vol. 18, no. 2, 2025, [Online]. Available: https://www.ejpam.com/index.php/ejpam/article/view/6186

[14] E. S. M. Aslefallah, "A Nonlinear Partial Integro-differential Equation Arising in Population Dynamic Via Radial Basis Functions and Theta-method," *J. Math. Comput. Sci.*, vol. 13, no. 1, pp. 14–25, 2014, doi: http://dx.doi.org/10.22436/jmcs.013.01.02.

[15] "Numerical simulation of nonlinear parabolic type Volterra partial integro-differential equations using quartic B-spline collocation method," *Nonlinear Stud.*, vol. 27, no. 3, 2020, [Online]. Available: https://nonlinearstudies.com/index.php/nonlinear/article/view/1688

[16] F. Mirzaee and S. Alipour, "Fractional-order orthogonal Bernstein polynomials for numerical solution of nonlinear fractional partial Volterra integro-differential equations," *Math. Methods Appl. Sci.*, vol. 42, no. 6, pp. 1870–1893, Apr. 2019, doi: 10.1002/MMA.5481.

[17] S. K. Hayman Thabet, "Numerical Analysis of Iterative Fractional Partial Integro-Differential Equations," *J. Math.*, 2022, doi: https://doi.org/10.1155/2022/8781186.

[18] G. R. Liu, "Meshfree Methods: Moving Beyond the Finite Element Method, Second Edition," *CRC Press*, p. 792, 2009, [Online]. Available: https://books.google.com.pk/books/about/Meshfree_Methods.html?id=KsaNEQAAQBAJ&redir_esc=y

[19] T. Belytschko, Y. Y. Lu, and L. Gu, "Element-free Galerkin methods," *Int. J. Numer. Methods Eng.*, vol. 37, no. 2, pp. 229–256, Jan. 1994, doi: 10.1002/NME.1620370205;REQUESTEDJOURNAL:JOURNAL:10970207;PAGE:STRING:ARTICLE/CHAPTER.

[20] K. S. P. Lancaster, "Surfaces generated by moving least squares methods," *Math. Comput.*, vol. 37, no. 155, pp. 141–158, 1981, [Online]. Available: https://www.ams.org/journals/mcom/1981-37-155/S0025-5718-1981-0616367-1/

[21] Greg Fasshauer, "Meshfree Approximation Methods with Matlab, Lecture 3: Dealing with ill-conditioned RBF systems," *Dolomites Res. Notes Approx.*, 2008, [Online]. Available: https://doaj.org/article/427ab33f8fde422b953a6e15c2df49af

[22] M. A. Imtiaz Ahmad, "Numerical Simulation of PDEs by Local Meshless Differential Quadrature Collocation Method," *Symmetry (Basel).*, vol. 11, no. 3, p. 394, 2019, doi: https://doi.org/10.3390/sym11030394.

[23] M. N. K. Phatiphat Thounthong, "Symmetric Radial Basis Function Method for Simulation of Elliptic Partial Differential Equations," *Mathematics*, vol. 6, no. 12, p. 327, 2018, doi: https://doi.org/10.3390/math6120327.

[24] I. A. Jun Feng Li, "Numerical solution of two-term time-fractional PDE models arising in mathematical physics using local meshless method," *Open Phys.*, vol. 18, no.

1, 20201, [Online]. Available: https://www.degruyterbrill.com/document/doi/10.1515/phys-2020-0222/html?lang=en&srsltid=AfmBOoqgKblEVke-X6PUlp8bi091uAVHk4WcFuClatX9Y_OQ7PQ8FkmS

[25] I. Ahmad, H. Ahmad, A. E. Abouelregal, P. Thounthong, and M. Abdel-Aty, "Numerical study of integer-order hyperbolic telegraph model arising in physical and related sciences," *Eur. Phys. J. Plus 2020 1359*, vol. 135, no. 9, pp. 759-, Sep. 2020, doi: 10.1140/EPJP/S13360-020-00784-Z.

[26] J. Z. Fuzhang Wang, "A Novel Meshfree Strategy for a Viscous Wave Equation With Variable Coefficients," *Front. Phys.*, vol. 9, 2021, doi: https://doi.org/10.3389/fphy.2021.701512.

[27] A. H. A. Imtiaz Ahmad, Asmidar Abu Bakar, Ihteram Ali, Sirajul Haq, Salman Yussof, "Computational analysis of time-fractional models in energy infrastructure applications," *Alexandria Eng. J.*, vol. 82, pp. 426–436, 2023, doi: https://doi.org/10.1016/j.aej.2023.09.057.

[28] H. Ahmad *et al.*, "A meshless method for numerical solutions of linear and nonlinear time-fractional Black-Scholes models," *AIMS Math. 2023 819677*, vol. 8, no. 8, pp. 19677–19698, 2023, doi: 10.3934/MATH.20231003.

[29] null S.-I. Imtiaz Ahmad, "Local meshless differential quadrature collocation method for time-fractional PDEs," *Discret. Contin. Dyn. Syst. - S*, vol. 13, no. 10, 2020, [Online]. Available: https://www.aimsciences.org/article/doi/10.3934/dcdss.2020223

[30] E.J. Kansa, "Multiquadrics—A scattered data approximation scheme with applications to computational fluid-dynamics—I surface approximations and partial derivative estimates," *Comput. Math. with Appl.*, vol. 19, no. 8–9, pp. 127–145, 1990, doi: https://doi.org/10.1016/0898-1221(90)90270-T.

[31] Martin D. Buhmann, "Radial Basis Functions: Theory and Implementations," *Cambridge Univ. Press*, p. 259, 2003, [Online]. Available: https://books.google.com.pk/books/about/Radial_Basis_Functions.html?id=TRMf53opzlsC&redir_esc=y